(Received 17 September 2025, Accepted 15 November 2025, Scheduled 12 December 2025)

Design and Analysis of High Isolation Four Port MIMO Antenna for N77 Band 5G Communication

Ramesh Manikonda[1,*], Govindarao Tamminaina[2], and Subhashini Gulla[3]

[1]Department of Electronics and Communication Engineering, GITAM University, Visakhapatnam, India
[2]Department of Electronics and Communication Engineering, MVGR College of Engineering, Visakhapatnam, India
[3]Department of Physics, SVP Engineering College, Visakhapatnam, India

ABSTRACT: This paper proposes a four-port multiple-input multiple-output (MIMO) antenna for 5G communication. The reference hexagonal antenna with WI-FI slots is designed on FR-4 substrate. Next, four reference antennas are arranged orthogonal to each other for the reduction of isolation. The overall dimensions of WI-FI slot four port MIMO antenna is $60 \times 60 \times 1.6\,\text{mm}^3$, and it is implemented on an FR-4 substrate with defective ground structure. With an impedance bandwidth of 1 GHz (Giga Hertz), the suggested MIMO antenna operates in the frequency range of 3.3 to 4.3 GHz. The mutual coupling is more than 23 dB among all ports. Furthermore, the MIMO antennas' channel capacity loss (CCL), diversity gain (DG), and envelope correlation coefficient (ECC) are estimated. The parameters are measured using anritsu MS2037C Vector Network Analyzer (VNA).

1. INTRODUCTION

A quad-element MIMO antenna [1], divided into four units for sub-6 GHz users, has been developed. The upper part of the setup features a 50 Ω microstrip monopole with unique openings in a defected ground structure, including semicircular and rectangular shapes. With dimensions of $60 \times 60 \times 1.6\,\text{mm}^3$, and this quad-element MIMO antenna offers impressive performance. To meet the demands of 5G applications, a compact four-element MIMO antenna solution [2] is recommended. Utilizing semicircular and rectangular monopole structures in an offset-fed configuration, the design achieves high isolation between adjacent elements without explicit isolation techniques. The manufactured antenna measures $0.374\lambda_0 \times 0.275\lambda_0$, with λ_0 denoting the 3.3 GHz free-space wavelength. With isolation exceeding 20 dB over the 3.3–6.3 GHz range, the antenna meets MIMO criteria for ECC, DG, and mean effective gain (MEG). A low-profile MIMO-5G in-vehicle antenna system [3], covering the whole 5G NR (New Radio) frequency spectrum is made of inexpensive printed circuit boards (PCBs). Designed for compactness using PCBs, this system includes a main 5G antenna and a two-part diversity antenna. Installed within a shark-fin enclosure on a vehicle roof, the system's dimensions are $0.1\lambda \times 0.07\lambda \times 0.14\lambda$, covering broad bands from 617–960 MHz and 1710–6000 MHz, supplemented with metal patches for high-frequency band coverage. A meander-line radiation arm design [4] is proposed for size reduction. Ring director is positioned above the aperture to produce stable radiation patterns and a broad impedance bandwidth. A MIMO antenna array [5] at 77 GHz with strong isolation and high gain is made up of two rows of transmitting and receiving antenna arrays. The TX (Transmitter) and RX (Receiver) antenna components have boresight gains more than 12 dBi, and their isolation at 75–81 GHz is about 42 dB. A two-port composite antenna [6] with tapered slots offers support dipole and W8JK array modes for co-linear polarization, with strong isolation of more than 20 dB in 3.4–4.1 GHz frequency band and low reported envelope correlation coefficients ($< 2.5 \times 10^{-3}$). A study on ultra-wideband (UWB)-MIMO antenna [7] explores a stepped electromagnetic bandgap (EBG) structure for a UWB-MIMO antenna, maximizing bandwidth while ensuring high isolation and radiation efficiency. It can cover 3.07–11.1 GHz while maintaining better isolation ($>$ 20 dB), radiation efficiency ($>$ 75%), and ECC ($<$ 0.05). A compact four-port wideband H and I slot MIMO antenna is employed for 5G purposes [8], and offering a −10 dB impedance bandwidth spanning 2.0 GHz, it resonates effectively from 3.4 GHz to 5.4 GHz. This antenna efficiently covers essential 5G NR bands including n77, n78, and n79, ensuring robust connectivity and compatibility with diverse network requirements. In [9], a design proposal for a 1×4 substrate integrated waveguide (SIW) based slot antenna is presented. Through careful adjustment of lateral wall positions and optimization of central wall and septum dimensions, the antenna achieves precise tuning of longitudinal and capacitive currents. This tuning helps the antenna to maintain a compact size of $9.8 \times 38.64 \times 0.508\,\text{mm}^3$, a minimum isolation of 30 dB, and a maximum gain of 10 dBi in the 36.5–39.28 GHz range.

In a recent study [10], a novel decoupling technique is proposed for an 8×8 MIMO array employing coupling stubs. The array features back-to-back connected printed Inverted-F antennas (PIFAs). Through complementary cancellation, significant reduction of coupling is achieved, resulting in isolation exceeding 10.2 dB from 3.3 to 4.88 GHz (38.6%). Another research endeavour [11] introduces a diamond-shaped MIMO

* Corresponding author: Ramesh Manikonda (rmanikon@gitam.edu).

antenna system tailored for 5G wireless communication. With compact dimensions of $26\times16\times0.254\,\text{mm}^3$, this system covers from 26.2 to 34.2 GHz frequency. Employing a two-element array configuration, the system experiences a gain increase from the single antenna element's 3.8 dBi to 7.6 dBi. It showcases robust MIMO capabilities with an envelope correlation value below 0.0005, a maximum DG of 10 dB, radiation efficiency above 90%, and 25 dB isolation. Additionally, [12] presents a slotted wideband eight-element MIMO antenna system catering to the N77 (3.2–4.2 GHz) requirements. Fabricated on an FR-4 substrate measuring $150\times75\,\text{mm}^2$ and 0.8 mm thick, the MIMO antennas incorporate an inverted C-slotted stub along with a T-slot to cover the 3.25–4.49 GHz frequency range. The addition of these slots boosts isolation to 14.5 dB and enables impressive performance metrics such as 40 bps/Hz channel capacity, DG exceeding 9.95 dB, and an ECC below 0.025. Furthermore, [13] deals with a four-element metamaterial MIMO antenna. Constructed on a compact square substrate measuring $50\times50\times1.6\,\text{mm}^3$ ($0.650\lambda_0\times0.65\lambda_0\times0.002\lambda_0$), where λ_0 denotes the 4 GHz free space wavelength, the antenna achieves significant reduction of mutual coupling between all ports by at least 23 dB. Additionally, [14] introduces an 8-panel huge MIMO antenna system utilizing a 4×4 phased antenna array capable of accommodating band combinations like n257/n261/n260 or n258/n260. This system offers a broad bandwidth of approximately 42.2% and boasts impressive features such as side lobes below 9.4 dB, a scanning range of $\pm40°$, and a minimum peak gain of 17 dBi. Through the implementation of a decoupling technique, neighbouring antenna elements are effectively isolated from each other by a minimum of 17 dB. In [15], unlike previous models utilizing an FSS structure solely for decoupling, this antenna ingeniously employs it as the direct low-band (LB) antenna at 0.69–0.96 GHz. Simultaneously, the FSS acts as a reflector for the high-band (HB) antennas within the range of 3.3–3.8 GHz. This innovative approach synchronizes the radiation patterns of both HB and LB antennas, resulting in stable radiation and significant gains in boresight across operational bands.

The performance of a large-scale multiuser MIMO millimetre wave (mm Wave) channel in an underground mine is examined in [16]. A base station operates at 28 GHz with 64 virtual antenna components catering to multiple customers, and the study highlights minimal time dispersion in the underground mine channel. Furthermore, it is noted that propagation distance does not notably affect the rms delay spread, showcasing a capacity potential of up to 33.54 bit/s/Hz with eight active users. The mode cancellation technique [17] is employed to reduce the MIMO-SAR (Specific Absorption Rate) by 82%. Through simulation and validation, the study presents an eight-antenna MIMO array greater than 16.7 dB of isolation, and efficiency surpassing 55% is produced. Polarisation diversity is produced on a dual-patch radiator [18] by excitation of various modes like TM_{20}, antiphase TM_{20} and TM_{01}. Based on this concept, a dual-element six-port MIMO antenna is developed, constructed, and tested, demonstrating an -6 dB impedance bandwidth between 4.8 and 5.0 GHz with more than 30 dB of isolation. In [19], partly reflecting surfaces (PRSs) are integrated to reduce mutual coupling. Operating over a bandwidth of 24–43.5 GHz (57.8%) at a -10 dB reflection coefficient, the antenna achieves transmission coefficients $|S_{21}|$, $|S_{31}|$, and $|S_{32}|$ less than 27, 37.9, and 46.4 dB, respectively, with maximum gains of 17.3 and 16.1 dBi. The unique design decoupling mechanism [20] is achieved by perpendicular bending of two slot antennas and introduction of a short-ended slot. Finally, [21] presents a tripolarized MIMO antenna with pattern diversity to achieve orthogonal polarization for each mode. By incorporating shorting pins and metal strips, the design achieves three adjacent resonant frequencies in patch mode, resulting in a wide bandwidth of 2.98–4.75 GHz with peak gains of 5.1 and 9 dBi.

The significance of attaining high isolation, small construction, and wideband performance for 5G applications is emphasized in this paper, which has a direct bearing on MIMO antenna design. To reduce mutual coupling and improve system performance, the suggested MIMO structure uses sophisticated design strategies such as element location optimization. Improved data speed, dependability, and spectral efficiency — all crucial for next-generation wireless systems — are guaranteed by the MIMO scenario's carefully placed antenna elements, which permit many independent communication channels.

2. METHODOLOGY OF QUAD PORT MIMO ANTENNA

2.1. Reference Antenna Design

Initially, the side length of the hexagonal patch is determined using the following equations and subsequently optimized to achieve improved performance values [30]. The antenna structure undergoes an evolution from a hexagonal patch to a novel configuration achieved by integrating four slots within the patch. In contrast to traditional rectangular or circular patches, the suggested single antenna element uses a hexagonal-shaped patch, which provides a compact geometry with effective surface current dispersion.

$$f_r = \frac{1.842C}{2\pi a\sqrt{\varepsilon_r}} \tag{1}$$

$$a_e = a\left\{1+\frac{2h}{\pi a\varepsilon_r}\left(\ln\frac{\pi a}{2h}+1.7726\right)\right\}^{1/2} \tag{2}$$

$$\pi a_e^2 = 3\sqrt{3}S^2 \tag{3}$$

f_r is the resonance frequency; c is velocity of light; a and a_e are radius and effective radius of circular patch; ε_r is the relative permittivity of substrate; h is the height of substrate; S is the side length of hexagonal patch. Single element antenna designed on an FR-4 substrate of 1.6 mm thickness, $\varepsilon_r = 4.4$, $\tan\delta = 0.02$, and its configuration depicted in Fig. 1(a) is of a basic hexagonal shape. Fig. 1(b) is hexagonal with four slots, and Fig. 1(c) is back view of the defective ground.

The antenna is fed with microstrip line and also uses partial ground to achieve impedance matching. Fig. 2(a) shows the S_{11} (dB) with and without slots of hexagonal antenna. The three arc slots are created on a hexagonal patch, and the current distribution is changed by slots. Due to these slots, the bandwidth is enhanced. The optimized hexagonal antenna design

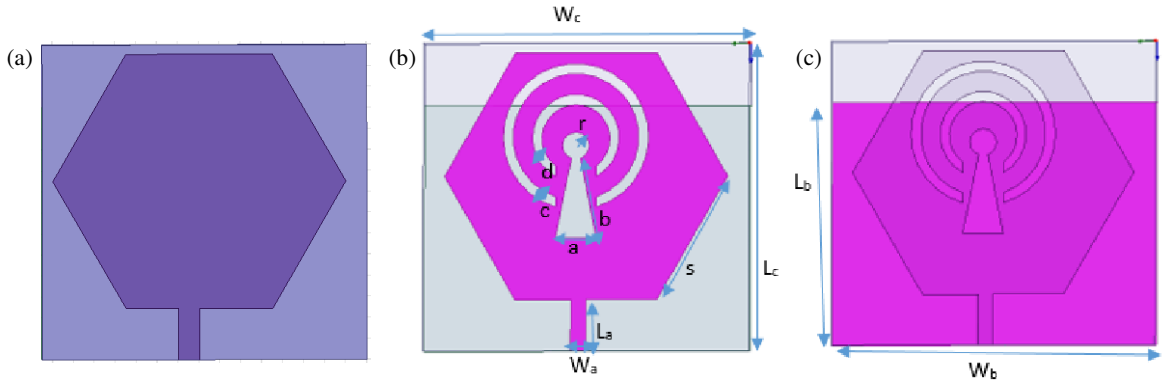

FIGURE 1. Schematic view of the reference antenna, (a) hexagonal, (b) hexagonal with slots, (c) back view.

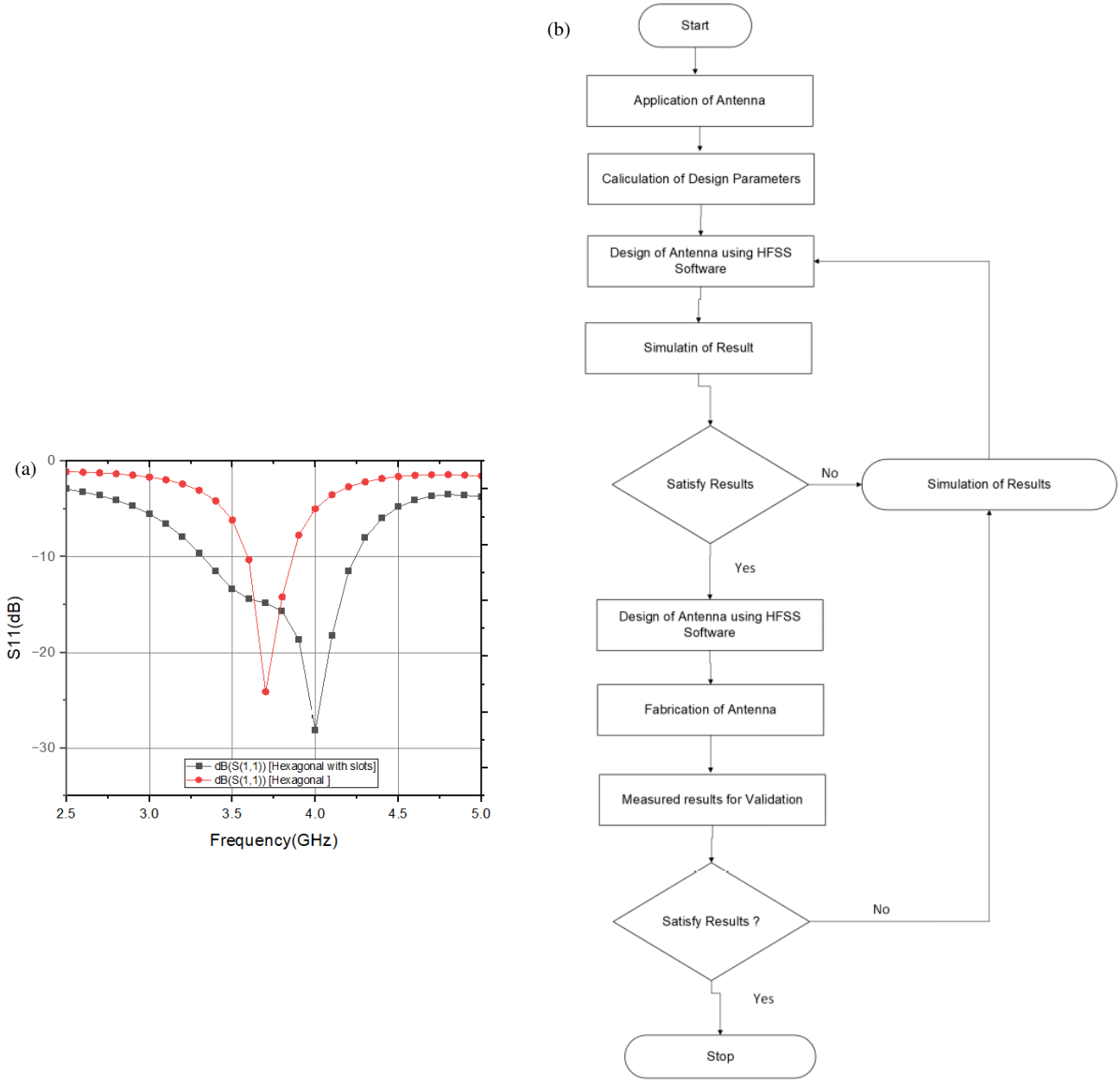

FIGURE 2. Reference antenna, (a) S_{11}, (b) flowchart.

TABLE 1. Design parameters of the reference antenna.

Parameter	S	L_c	W_c	L_a	W_a	a	b	c	d	r	L_b	W_b
Value (mm)	14	30	30	4.9	1.5	4	8	1	1	1.3	24	30

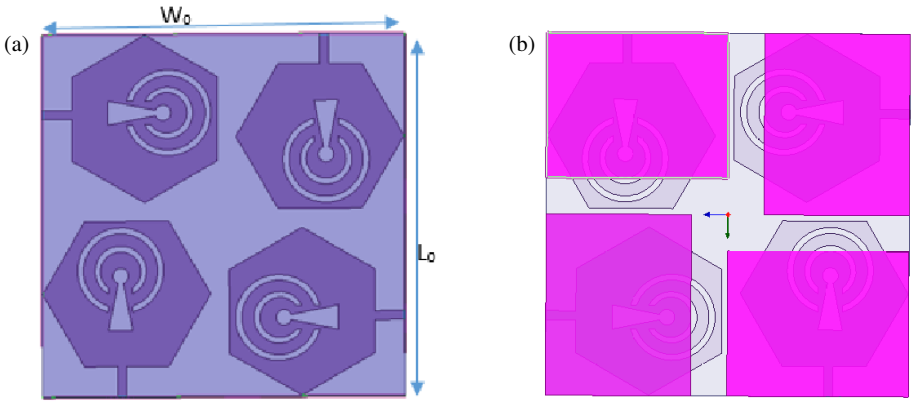

FIGURE 3. Schematic view of MIMO antenna, (a) front, (b) back view.

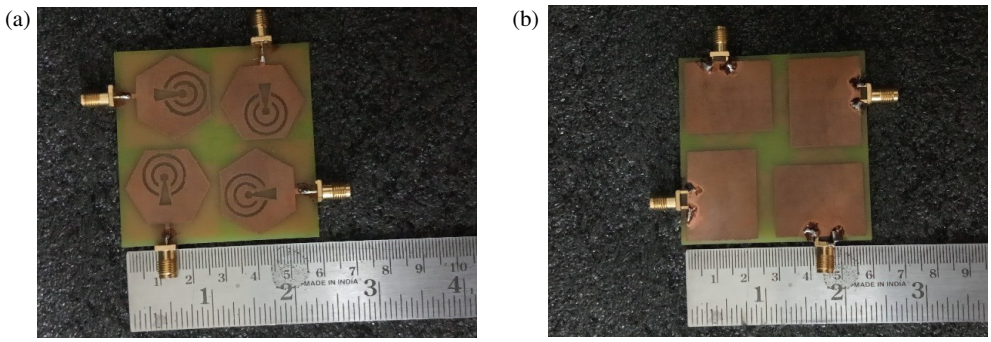

FIGURE 4. Fabrication of MIMO antenna, (a) front, (b) back view.

with WI-FI slots is chosen, and it enhances the bandwidth, operating throughout the desired frequencies from 3.3 to 4.3 GHz. Table 1 gives dimensions of the single hexagonal antenna with slots. Fig. 2(b) shows the flowchart of proposed MIMO antenna.

2.2. Design of MIMO Antenna

Figures 3(a) and 3(b) illustrate the schematic front and back views of the quad-port MIMO antenna. This antenna is built using an FR-4 substrate measuring 1.6 mm in thickness incorporating a defective ground structure. The four reference antennas are arranged orthogonally to each other within the design. The final dimensions of the proposed antenna are 60 mm in width (W_o) and 60 mm in length (L_0). In Figs. 4(a) and 4(b), the fabrication details of the MIMO antenna are presented. The antenna is simulated with High Frequency Structure Simulator (HFSS) software.

3. RESULTS AND DISCUSSIONS

This section provides a thorough description while also explaining the outcomes of a four port MIMO antenna. Isolation, ECC, DG, and CCL are among the MIMO antenna properties that are simulated/measured. Fig. 5(a) shows the reflection coefficients (S_{11}, S_{22}, S_{33}, and S_{44}) of MIMO antenna at four different ports 1, 2, 3, and 4. All the reflection coefficients of MIMO antenna are from 3.3 to 4.3 GHz. Fig. 5(b) depicts the measured and simulated reflection coefficients of proposed MIMO antenna at port 1. It resonates from 3.3 to 4.3 GHz with impedance bandwidth 1 GHz, and max reflection coefficient is -28.0 dB at 4 GHz.

Here, the measured lower cut-off of S_{11} is varied due to SMA connector. The reflection coefficient (S_{11}) of the proposed MIMO antenna was measured using ANRITSU MS2037C VNA. Fig. 6 illustrates both the measured and simulated transmission coefficients of the WI-FI slot MIMO antenna. Notably, within the proposed frequency band of 3.3–4.3 GHz, the isolation value remains below 23.0 dB. This enhanced isolation is attributed to the orthogonal positioning of the four reference antennas.

Given its significance as a primary performance metric for MIMO antenna systems [22, 23], the ECC can be calculated utilizing the provided equation and S-parameters. The parameters

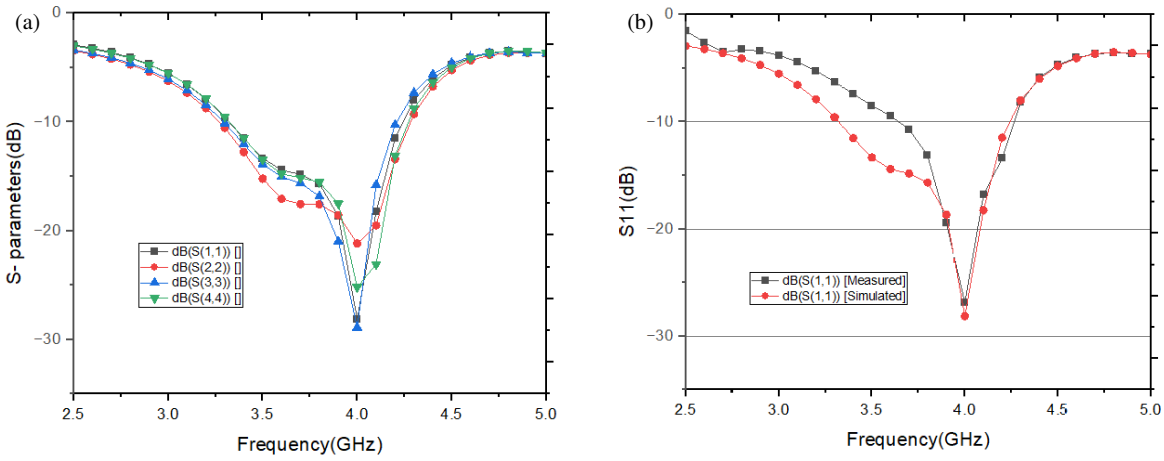

FIGURE 5. S-parameters of MIMO antenna at (a) four ports, (b) measured S_{11}.

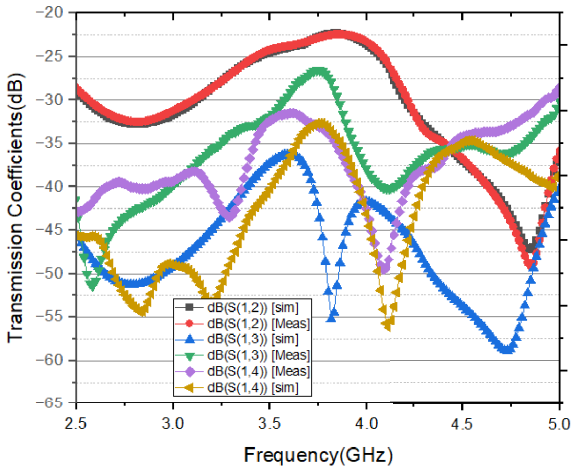

FIGURE 6. Transmission coefficients of four port MIMO antenna.

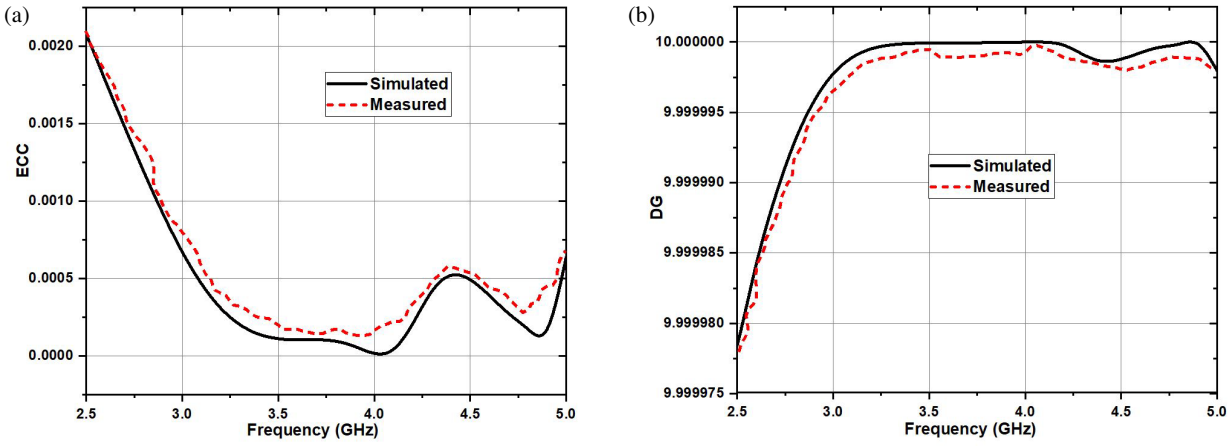

FIGURE 7. Four port MIMO antenna measured/simulated (a) ECC, (b) DG.

i and j in Equation (1) represent the port number.

$$\mathrm{ECC} = \frac{\left|S_{ii} * S_{ij} + S_{ji} * S_{jj}\right|^2}{\left(1 - \left|S_{ii}\right|^2 - \left|S_{ji}\right|^2\right) * \left(1 - \left|S_{jj}\right|^2 - \left|S_{ij}\right|^2\right)} \quad (4)$$

In order to preserve the wireless system's quality and dependability, the MIMO antenna's diversity gain (DG) needs to be strong. Additionally, it is computed by

$$\mathrm{DG} = 10\sqrt{1 - (\mathrm{ECC})^2} \quad (5)$$

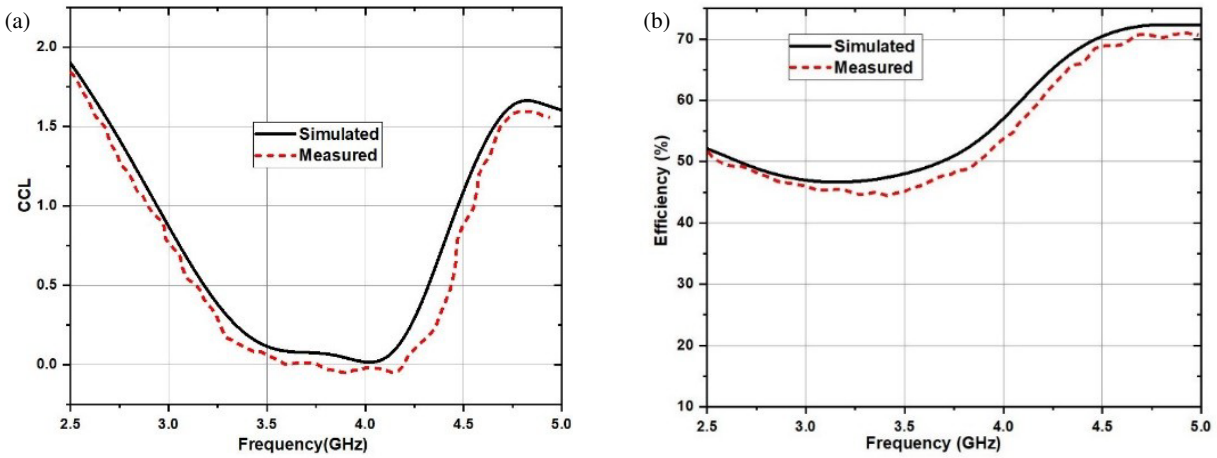

FIGURE 8. Four port MIMO antenna, (a) CCL, (b) radiation efficiency.

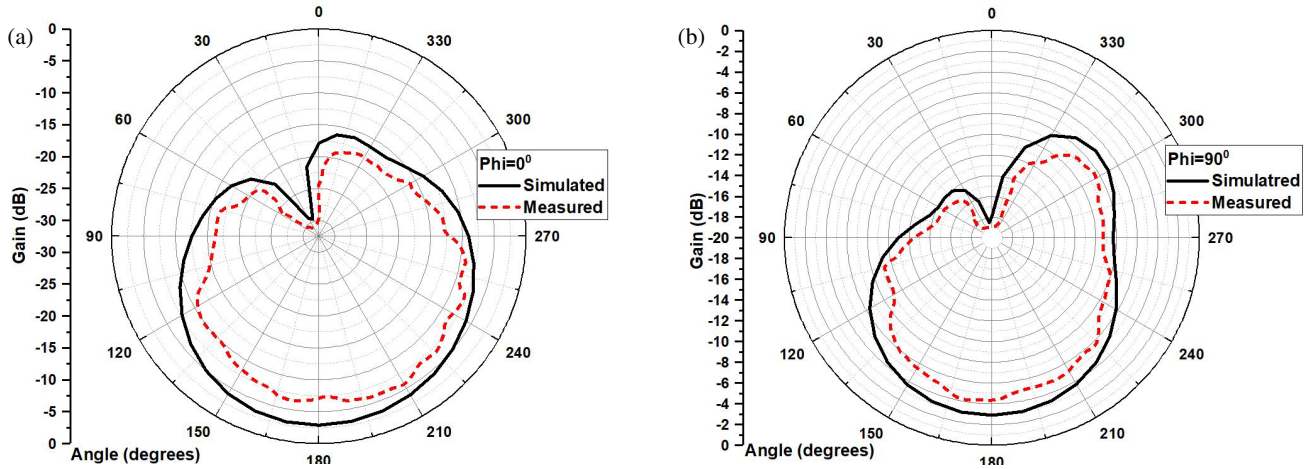

FIGURE 9. Radiation pattern of four port MIMO antenna at (a) phi $= 0°$, (b) phi $= 90°$.

One further crucial characteristic for the MIMO system is channel capacity loss (CCL), which should have a value of less than 0.4 bits/s/Hz. Using this formula to determine capacity loss,

$$\text{CCL} = -\log_2(\varphi^R) \tag{6}$$

Here, φ^R is the correlation matrix of the receiving antenna, expressed as follows.

$$(\varphi^R) = \begin{matrix} \varphi_{ii} & \varphi_{ij} \\ \varphi_{ji} & \varphi_{jj} \end{matrix} \tag{7}$$

Here, $\varphi_{ii} = 1 - (|S_{ii}|^2 + |S_{ij}|^2)$, $\varphi_{jj} = 1 - (|S_{jj}|^2 + |S_{ji}|^2)$, $\varphi_{ij} = -(S_{ii}{*}S_{ij}+S_{ji}{*}S_{jj})$ and $\varphi_{ji} = -(S_{jj}{*}S_{ji}+S_{ij}{*}S_{ii})$.

The measured and simulated EEC values are less than 0.0005 for a desired frequency band, shown in Fig. 7(a). Also, diversity gain is above 9.99 dB of the WI-FI slot four port MIMO antenna, shown in Fig. 7(b). Fig. 8(a) shows that the CCL is less than 0.3, and Fig. 8(b) shows the radiation efficiency between 48 and 61% for the proposed frequency range of quad MIMO antenna.

Figure 9 illustrates the radiation pattern of the quad-port WI-FI slot MIMO antenna at $\varphi = 0°$ and $\varphi = 90°$ for 4.0 GHz, as shown in Fig. 9(a) and Fig. 9(b), respectively. Additionally, Fig. 10 presents the surface current distribution at 4.0 GHz, with the maximum current concentrated around the feed line and slots. The 4.0 GHz simulated surface current distribution makes it abundantly evident that when one element is excited,

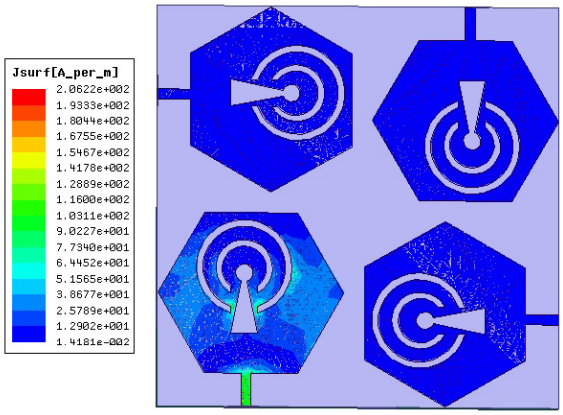

FIGURE 10. Current distribution of four port MIMO antenna.

TABLE 2. Comparison of MIMO parameters.

Ref.	Bandwidth (GHz)	Decoupling	Efficiency (%)	Isolation (dB)	No. of ports	ECC
[24]	3.4–3.6	No	40–52	> 10	8	< 0.15
[25]	3.3–3.6	Yes	45–60	> 15	8	< 0.15
[26]	3.4–3.6	No	38–64	> 12	4	< 0.13
[27]	3.9–5.2	No	80–84	> 15	6	< 0.002
[28]	3.0–4.8	No	NA	> 17	4	< 0.01
[29]	3.2–3.8	Yes	NA	> 16	4	< 0.07
Pro. Ant.	3.3–4.3	No	48–60	> 23	4	< 0.0005

the resulting strong localized currents are limited to that patch and the surrounding ground region, while the induced currents of the orthogonally positioned adjoining elements are negligible. This demonstrates how well the orthogonal arrangement inhibits mutual coupling and surface-wave propagation, improving isolation and MIMO performance. For a comparative analysis, Table 2 provides a comparison of the proposed MIMO antenna with other antennas.

4. CONCLUSION

The paper presents four port Hexagonal with WI-FI shaped slots MIMO antenna, and it is suitable for sub-6 GHz 5G mobile applications. The proposed MIMO antenna resonates within the frequency range of 3.3 to 4.3 GHz, offering an impedance bandwidth of 1 GHz, thereby covering the N77 band. The diversity gain is above 9.99 dB, CCL less than 0.3, and ECC less than 0.0005 for the proposed frequency band (3.3 to 4.3 GHz). The max radiation efficiency is 60%. The isolation is 23.0 dB for the desired frequency band due to orthogonality. The measured results closely match simulated ones.

REFERENCES

[1] Abhilash, A., P. Thomas, K. K. Indhu, K. Neema, R. A. Kumar, and C. Aanandan, "Four-element compact and dual-band MIMO antenna with self-decoupled mechanism for 5G applications," *Progress In Electromagnetics Research C*, Vol. 123, 91–99, 2022.

[2] Verulkar, S. M., A. Khade, M. A. Trimukhe, and R. K. Gupta, "Compact wideband four elements MIMO antenna for 5G applications," *Progress In Electromagnetics Research C*, Vol. 137, 199–209, 2023.

[3] Zhou, Y., T. Jiang, H. Li, and F. Chen, "A 5G MIMO multiband low-profile antenna design for automotive shark-fin systems," *IEEE Antennas and Wireless Propagation Letters*, Vol. 23, No. 5, 1588–1592, 2024.

[4] Feng, Y., Y. Chen, and L. Cao, "A compact base station MIMO antenna array with miniaturized antenna elements," *IEEE Transactions on Circuits and Systems II: Express Briefs*, Vol. 71, No. 2, 607–611, Feb. 2024.

[5] Yan, S., Q. Chen, X. Guo, Z. Qiao, Q. Yang, S. Feng, Z. Huang, L. Yang, and Y. Li, "A high-isolation high-gain MIMO millimeter-wave antenna array," *IEEE Transactions on Antennas and Propagation*, Vol. 72, No. 2, 1201–1211, 2024.

[6] Gao, R. B., L. Y. Nie, F. Cheng, Z. N. Jiang, X. H. Zhang, and S. Xiang, "A wideband colinearly polarized composite antenna with high isolation," *IEEE Antennas and Wireless Propagation Letters*, Vol. 23, No. 1, 419–423, Jan. 2024.

[7] Li, W., L. Wu, S. Li, X. Cao, and B. Yang, "Bandwidth enhancement and isolation improvement in compact UWB-MIMO antenna assisted by characteristic mode analysis," *IEEE Access*, Vol. 12, 17 152–17 163, 2024.

[8] Tamminaina, G. and R. Manikonda, "Design and analysis of wideband four-port multiple input multiple output antenna using defective ground structure for 5G communication," *International Journal of Electrical and Computer Engineering (IJECE)*, Vol. 14, No. 2, 1646–1653, 2024.

[9] Singh, A. K. and S. Pal, "Compact self-isolated extremely low ECC folded-SIW-based slot MIMO antenna for 5G application," *IEEE Antennas and Wireless Propagation Letters*, Vol. 23, No. 1, 194–198, Jan. 2024.

[10] Wen, L., M. Zhang, W. Hu, Q. Yang, and W. Xiao, "Coupling cancellation using coupling stubs for MIMO array applications," *IEEE Antennas and Wireless Propagation Letters*, Vol. 23, No. 1, 204–208, Jan. 2024.

[11] Raheel, K., A. W. Ahmad, S. Khan, S. A. A. Shah, I. A. Shah, and M. Dalarsson, "Design and performance evaluation of orthogonally polarized corporate feed MIMO antenna array for next-generation communication system," *IEEE Access*, Vol. 12, 30 382–30 397, 2024.

[12] Kiani, S. H., M. E. Munir, H. S. Savci, H. Rmili, E. Alabdulkreem, H. Elmannai, G. Pau, and M. Alibakhshikenari, "Dual-polarized wideband 5G N77 band slotted MIMO antenna system for next-generation smartphones," *IEEE Access*, Vol. 12, 34 467–34 476, 2024.

[13] Khan, I., K. Zhang, L. Ali, and Q. Wu, "Enhanced quad-port MIMO antenna isolation with metamaterial superstrate," *IEEE Antennas and Wireless Propagation Letters*, Vol. 23, No. 1, 439–443, Jan. 2024.

[14] Chaudhari, A. D. and S. Mukherjee, "Exploiting the viability of antenna arrays for multi-band FR2 base-station massive MIMO systems," in *2024 16th International Conference on Communication Systems & Networks (COMSNETS)*, 1143–1147, Bengaluru, India, 2024.

[15] Li, H., J. Xu, Y. Nan, Q. Chen, and C. Zhou, "Low-profile dual-band shared-aperture base station antennas based on FSS radiators," *IEEE Antennas and Wireless Propagation Letters*, Vol. 23, No. 6, 1894–1898, 2024.

[16] Hadji, S. E., M. Nedil, M. L. Seddiki, and I. B. Mabrouk, "Millimeter-wave massive MU-MIMO performance analysis for private underground mine communications," *IEEE Transactions on Antennas and Propagation*, Vol. 72, No. 2, 1792–1803, Feb.

2024.

[17] Fang, Y., Y. Jia, J.-Q. Zhu, Y. Liu, and J. An, "Self-decoupling, shared-aperture, eight-antenna MIMO array with MIMO-SAR reduction," *IEEE Transactions on Antennas and Propagation*, Vol. 72, No. 2, 1905–1910, Feb. 2024.

[18] Qian, L., X. Chen, H. Zhou, H. Wang, and M. Hou, "Tri-mode dual-patch MIMO antenna with high isolation for 5G terminal applications," *IEEE Transactions on Antennas and Propagation*, Vol. 72, No. 2, 1953–1958, Feb. 2024.

[19] Li, Q., S. Liao, Y. Yang, Z. Liang, and S. Xiao, "Wideband 5G millimeter-wave MIMO magnetoelectric dipole antenna integrated with partially reflective surfaces," *IEEE Transactions on Antennas and Propagation*, Vol. 72, No. 1, 445–453, Jan. 2024.

[20] Yuan, X., C. Huang, J. Sui, Y.-F. Cheng, X. Fang, and X. Zhu, "Wideband self-decoupled slot MIMO antennas with two transmission zeros," *IEEE Antennas and Wireless Propagation Letters*, Vol. 23, No. 1, 99–103, Jan. 2024.

[21] Yang, Y., J. Ren, B. Zhang, J. Liu, H. Wang, D. Song, and Y. Yin, "Wideband tripolarized MIMO antenna with pattern diversity for 5G application," *IEEE Antennas and Wireless Propagation Letters*, Vol. 23, No. 1, 349–353, Jan. 2024.

[22] Megahed, A. A., M. Abdelazim, E. H. Abdelhay, and H. Y. M. Soliman, "Sub-6 GHz highly isolated wideband MIMO antenna arrays," *IEEE Access*, Vol. 10, 19 875–19 889, 2022.

[23] Haque, M. A., M. S. Ahammed, S. Socheatra, R. A. Ananta, M. J. H. Nirob, N. S. S. Singh, N. M. Jizat, S. Alsowail, and S. S. Al-Bawri, "Machine learning based compact MIMO antenna array for 38 GHz millimeter wave application with robust isolation and high efficiency performance," *Results in Engineering*, Vol. 25, 104006, 2025.

[24] Wong, K.-L., C.-Y. Tsai, and J.-Y. Lu, "Two asymmetrically mirrored gap-coupled loop antennas as a compact building block for eight-antenna MIMO array in the future smartphone," *IEEE Transactions on Antennas and Propagation*, Vol. 65, No. 4, 1765–1778, 2017.

[25] Jiang, W., B. Liu, Y. Cui, and W. Hu, "High-isolation eight-element MIMO array for 5G smartphone applications," *IEEE Access*, Vol. 7, 34 104–34 112, 2019.

[26] Chang, L., Y. Yu, K. Wei, and H. Wang, "Polarization-orthogonal co-frequency dual antenna pair suitable for 5G MIMO smartphone with metallic bezels," *IEEE Transactions on Antennas and Propagation*, Vol. 67, No. 8, 5212–5220, 2019.

[27] Kumar, A., J. Mohanty, P. Pattanayak, D. Sabat, and G. Prasad, "Six-port mid-bands low-SAR MIMO antenna for WLAN, 5G mobile terminals, and C-band applications," *AEU — International Journal of Electronics and Communications*, Vol. 166, 154665, 2023.

[28] Muhsin, M., A. L. Nurlaili, A. Saharani, and I. R. Utami, "Sectoral dual-polarized MIMO antenna for 5G-NR band N77 base station," *Indonesian Journal of Electrical Engineering and Computer Science*, Vol. 21, No. 3, 1611–1621, 2021.

[29] Yu, Z., L. Huang, Q. Gao, and Y. Chen, "A compact microstrip four port dual circularly polarized MIMO antenna for sub-6G application," *Progress In Electromagnetics Research C*, Vol. 119, 145–159, 2022.

[30] Singh, K., S. Patil, A. Naik, and S. Kadam, "Hexagonal microstrip patch antenna design for UWB application," *ITM Web of Conferences*, Vol. 44, 02004, 2022.